Bulletin of Earth Sciences of Thailand

Reservoir Flow Unit Definition from Unit-Specific Permeability Estimates Using Wireline Logs and Core Data

Nuttapol Junput*

Petroleum Geoscience Program, Department of Geology, Faculty of Science,
Chulalongkorn University, Bangkok 10330, Thailand
*Corresponding author email: nuttapolj.1993@gmail.com

Abstract

Permeability is most the useful petrophysical property for guiding reservoir flow performance. In the Pattani Basin, Gulf of Thailand, the perforation strategy is complicated and requires accurate petrophysical property measurements in the reservoir in order to design the most effective perforation program. Factors that control reservoir permeability in Pattani Basin are not well understood, so currently there is no accurate method to predict and calculate the reservoir permeability in non-cored intervals in wells in Gulf of Thailand. In this study, the aim is to broaden a permeability prediction approach across a large area in the southern Pattani Basin with broad variations in depositional parameters. The results show different trends with different permeability prediction equations for each depositional facies. There are four facies defined by using the differences of lithology, based on sedimentary structures and depositional environments in the reservoirs namely a.) Conglomerate and conglomeratic sandstone b.) Fining-upward, cross-bedded sandstone c.) Interbedded sandstone and siltstone d.) Coarsening-upward, alternating sandstone and siltstone. The permeability prediction equation matches to raw data from core study have a coefficient of determination rank from 0.57 to 0.75, with an overall coefficient of determination of 0.81. The results from prediction equations calibrated between predicted permeability values and actual permeability values show an overall coefficient of determination of 0.40. Actual production performance validation shows an overall success rate of permeability prediction when using the study equations is 56.82%. The predicted permeability can be used to guide for the sequence of perforation and also guide perforation locations in the reservoir sands.

Keywords: Permeability Prediction, Southern Pattani Basin, Gulf of Thailand

1. Introduction

In the Pattani Basin, Gulf of Thailand, the perforation strategy is complicated and requires accurate petrophysical property measurements in the reservoirs in order to design the perforation program. Permeability is most the useful petrophysical property for guiding reservoir flow performance. Factors that control reservoir permeability in Pattani Basin are not well understood, so currently there is no accurate method to predict and calculate the reservoir permeability in non-cored intervals in wells in Gulf of Thailand.

Previous studies, focused on the Ubon area, used wireline logs and core data combined with an understanding of the depositional environment to create a local permeability prediction model (Chaiwan, 2010). The model predicts permeability values based on measurements in the cored section and applies this to well intervals in the non-cored section, mostly in wells that have core data. These studies have proven successful when the core-plug based permeability prediction model is applied in the same well and the outcome can be representative of whole sand body capacity (as confirmed by well test validation).

In this study, the aim is to broaden this approach across a larger area of the Pattani Basin showing more variation in depositional parameters. The objective of the study is to better understand factors controlling reservoir permeability, then predict the reservoir permeability by transforming wireline logs using core data and so generate the best permeability model to estimate reservoir flow unit properties and expand the cored to non-cored well prediction (with well test validation) across the whole southern area of Pattani Basin.

2. Methodology

Integrated wireline logs and core data, including petrographic studies, are the main information set used in this study. Conventional

cores from six wells (Figure 1) with petrographic data, were used to describe the reservoir facies types, based on detailed core data study and analysis of reservoir properties, especially permeability, so defining factors that control the reservoir quality. These were all integrated with wireline logs, which consists of gamma-ray, resistivity, neutron, density, shale volume, porosity and water saturation curves, to generate a permeability model from cored wells and so predict reservoir permeabilities in non-cored wells. Predictions are tested using actual reservoir production performance measures from 44 single perforated sands.

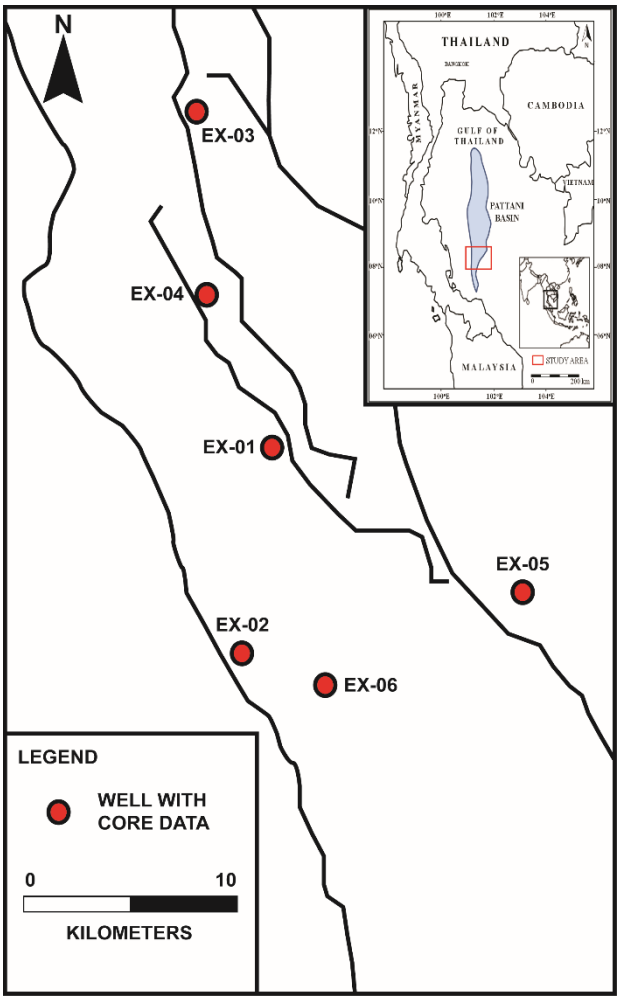

Figure 1 The study area is located in the southern part of Pattani Basin, and the location of the wells used in the study are shown.

3. Geological Overview

The Pattani Basin is a Tertiary rift basin, approximately 270 kilometers long and 100 kilometers wide (Watcharanantakul and Morley, 2000). It is characterized by a series of elongated north-south trending faults. The main structural styles are graben or half-graben, which are controlled by strike-slip faults in two dominant directions; NW-SE and NE-SW.

Pattani Basin, the largest basin in the Gulf of Thailand, has accumulated more than 8,000 meters of sediment since the Oligocene. It contains both non-marine and marginal-marine siliciclastic sediments (Jardine, 1997). Chevron Thailand Exploration and Production, Ltd., breakout the stratigraphy in the Gulf of Thailand and its fill into six lithostratigraphic units (Figure 2).

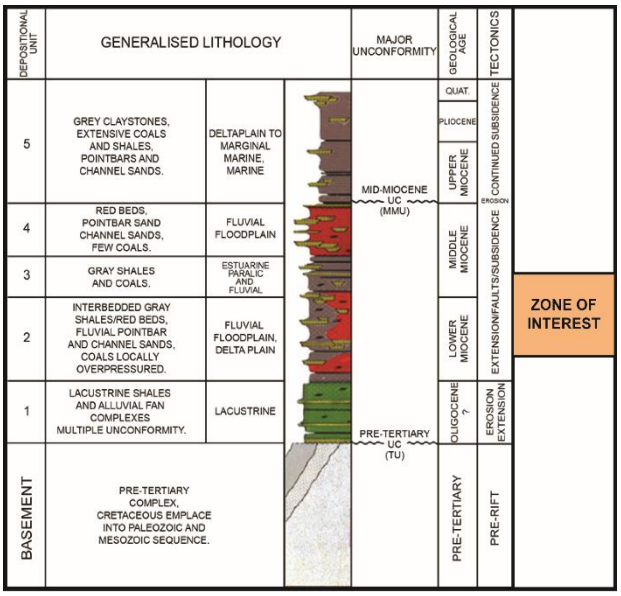

Figure 2 The stratigraphy of Pattani Basin, Gulf of Thailand (modified from Jardine, 1997). The study section covers the interval between the Lower and Middle Miocene.

The section of interest for this study covers interval from the lower part of Sequence 3 to the middle of Sequence 2. Sequence 2 is dominated by fluvial point-bar and channel deposits in the northern and central Pattani Basin (Jardine, 1997) and by upper intertidal, fluvial, and lower deltaic plain sediments in the southern basin (Lockhart et al., 1997). Lithologically, it is comprised of Lower Miocene variegated, dark-brown to reddish-brown claystones and grey to clear, fine to coarse-grained sandstones, with occasional

lignite seams and lenses. Sequence 3 is a succession of coastal plain, mangrove, swamp marginal-marine, and upper intertidal to subtidal lagoonal environments, made up of light to brownish grey claystone, mudstone with interbeds of sandstone, argillite and coal seams.

4. Facies Characterization

In a reservoir sand facies study, stratigraphic units are divided into two main lithofacies, reservoir facies, and non-reservoir facies (their associated facies). The facies division is based on conventional core description and interpretation, integrated with petrophysical properties and wireline log characteristics within the cored interval.

RESERVOIR FACIES

The reservoir facies are conglomerate and conglomeratic sandstone, fining-upward cross-bedded sandstone, interbedded sandstone and siltstone, and coarsening-upward alternating sandstone and siltstone.

Conglomerate and conglomeratic sandstone is made up of mudstone pebble conglomerate and conglomeratic sandstone that contain 1-40% rounded to angular mudstone pebbles clasts in moderately to poorly sorted, coarse to medium grained sandstone. The size of mudstone pebble clasts ranges from 5 mm to more than 140 mm in length. Conglomerate and conglomeratic sandstone, with moderately to poorly sorting, indicates high-energy deposition (fluvial bed-load deposition) in a unidirectional current. This interpretation is supported by the basal erosional contacts and the nature of mud clasts. Thick basal mudstone clast conglomerate overlain by coarse to medium grained sandstone may represent deposition in a coarse-grained, low-sinuosity meander belt or represent a time during which large amounts of sand were being brought into the basin by high-energy streams.

The upward-fining sandstones are made up of mostly medium to fine grained, moderately well sorted to poorly sorted, mostly moderately sorted sandstones. The facies comprises both single and multiple upward-fining sandstones stacks. Sandstones contain mostly small to medium scale cross laminations of mostly tough type, that occur in 0.3-2.0 ft thick sets. Cross laminations are defined by mica and coal rich layers that are 1-5 mm thick. Ripple cross lamination, wavy and parallel lamination are rare, and mostly occur in the upper part of this facies. The upward-fining successions indicate and upward decrease of energy. The interpretation is supported by grain size profiles that grade upward from medium to very fine grained sand and is also supported by a predominance of cross stratification and cross laminations in the lower part, and current-ripple laminations in the upper part of the facies. The dominance of trough cross strata integrated with geological settings, as described earlier, suggests these sandstones were deposited in fluvial channel system.

Interbedded sandstone and siltstone are made up of silty sandstones to clayey siltstones that tend to be very fine grained to silty at the top, with moderate to poor sorting. Overall, they tend to be fining-upward successions with sandstone beds become thinner upward. Silty zones at top generally contain micas and coaly particles. Dominant sedimentary structures are parallel lamination and ripple cross lamination (micro cross lamination). Sandstones interbedded with siltstones tend to occur in the upper parts of cross-bedded sandstones and are included within an overall-fining upward succession. Sandstone beds becoming thinner upward. The combination of features indicate sediments were deposited in currents with velocities and energies decreasing upward with passage from cross-bedded sandstones. The suspended sediment load, that deposits on the top of this facies, indicates deposition in low-energy environments. The interstratified silty sandstones, that overlie fluvial channel sandstones, contain probable root traces, burrows and soft sediment deformation structures suggesting this facies was deposited in fluvial channel levees and levees to floodplain transitional environments.

The upward-coarsening sandstones and siltstone unit is made up of mostly fine to very fine grained, silty, poorly sorted to very poorly sorted, with rare zones of moderately sorted, lower fine-grained sandstones, that are typically

silty in the basal part. Overall, the unit tends to be a coarsening-upward succession, as sandstone beds become thicker upward. Sandstones and siltstones are interlaminated at the 1 mm to 2 cm scale. Stratification consists of parallel, wavy and ripple laminations (both current and combined flow types are present). The upward-coarsening successions indicate an increase in energy upward. The interpretation is supported by the observation that the sandstone beds become thicker upward and the grain size profile grades upward from silty to fine grained sediments. Common sedimentary features are ripple lamination, parallel and wavy lamination, including flaser bedding with internal mud drapes, which are likely an indication of tidal influence. The common presence of burrows and bioturbation also implies these sandstones were deposited in a marine-influenced environment. Narapan (2015) suggests that this facies is an estuarine sand deposit and may relate to progradation of small sandstone layers (1.8 to 10 ft thickness), in a bay-head delta prograding into a shallow estuary.

NON-RESERVOIR FACIES

Associated facies include non-marine and marginal-marine facies. Non-marine deposition facies are mudstone, siltstone and coaly facies, interpreted as deposits of alluvial-plain flood basins, bays or lakes, abandoned channels, natural levees, and swamps. Additionally, marginal-marine depositional facies are claystone, mudstone, siltstone, and coaly facies, interpreted as bay or estuary deposits.

5. Petrographic Study of Reservoir Facies

All of the examined core plug end trims are sandstones. The grain size ranges from silt to lower very-coarse grained with the average grain size varying from upper very fine to lower coarse grained. The sandstones are mainly moderate to moderately well sorted. Grain angularity ranges from angular to subrounded and grain sphericity ranges from elongate to spherical. These samples are mainly classified as sublitharenite, feldspathic litharenite, subarkose and litharenite (with rare lithic arkose and quartzarenite) (Figure 3).

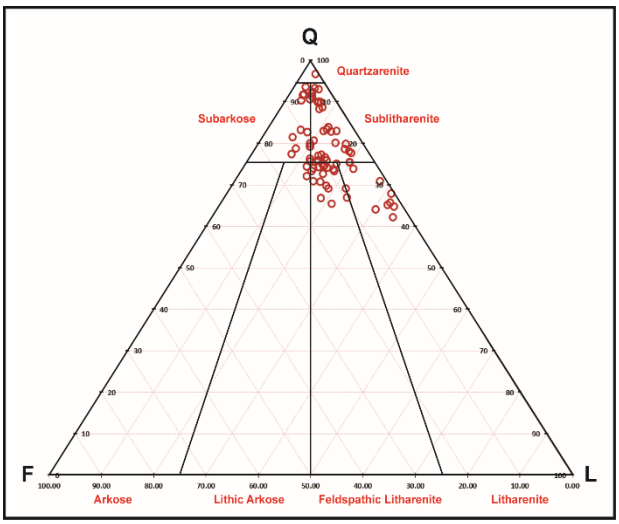

Figure 3 Sandstone classification of reservoir facies (Folk, 1974) plot of all available wells shows sandstone in this area is mainly classified as sublitharenite and feldspathic litharenite.

The framework grains are mostly quartz with minor to common feldspar and minor to very common lithic fragments. Accessory grains are detected in trace to minor amounts. Quartz consists of predominantly monocrystalline quartz, commonly displaying both undulose and straight extinction. Minor to common polycrystalline quartz is generally observed in all samples. Feldspars in this sample suite are commonly degraded and most are partially leached. Generally, untwinned potassium feldspar is the main type of feldspar observed. Lithic fragments are dominated by metamorphic rock fragments, mostly metaquartzite and lesser phyllitic fragments followed by chert, plutonic rock fragments, and sedimentary rock fragments. Accessory grains include trace to minor muscovite, heavy minerals (such as tourmaline and zircon), clay-replaced grains and carbonate-replaced grains.

Total authigenic cement content ranges from minor to abundant. Cements identified in these sandstones are calcite (mainly ferroan), dolomite, siderite, quartz overgrowths, pyrite, kaolinite, and pore-lining to pore-filling undifferentiated clay.

A generalized paragenetic sequence based on observable textural relationships of major authigenic cements and other diagenetic events is presented in Figure 4. The diagenetic sequence is arranged in approximate chronological order, although some overlapping of diagenetic processes may occur, and features documented below do not necessarily occur in all the samples.

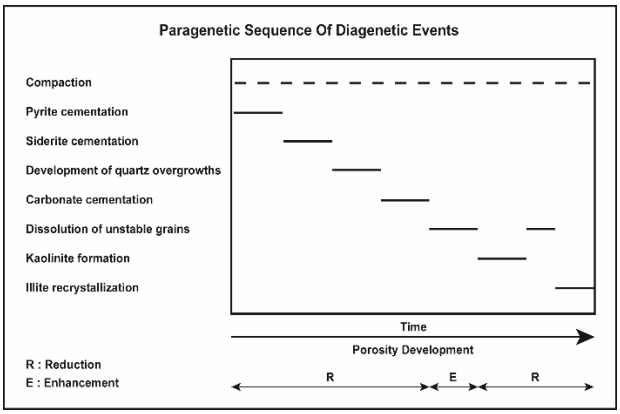

Figure 4 A generalized paragenetic sequence based on observable textural relationships of major authigenic cements and other diagenetic events (modified from Ejan et al., 1994).

In this suite of samples, total clay matrix as indicated by thin section modal analysis, ranges from trace to abundant. Clay matrix is divided into detrital dispersed, detrital laminar, and pseudomatrix. From scanning electron microscopy, dispersed clays are dominated by authigenic kaolinite, with lesser illite and mixed-layer illite/smectite. Authigenic kaolinite exhibits moderately to well developed crystals, mainly in booklet form. Illitic clay displays various morphologies include flaky, crenulated, hair-like and filamentous forms. Total clay content from X-ray diffraction analysis, varies from minor (1.0 wt. %) to abundant (40.4 wt. %). Clay fraction XRD analyses show kaolinite and mixed-layer illite/smectite to be the dominant clay mineral (kaolinite with an average of 36.5% of clay fraction and mixed-layer illite/smectite with an average of 32.3% of clay fraction with 20% expandable smectite interlayers) followed by illite (with an average of 20.8% of clay fraction), and chlorite (with an average of 10.4% of clay fraction).

Based on the visible porosity and pore interconnectivity observed in thin section, the reservoir quality of the sandstone samples appears to be very poor to very good. Pores are mostly secondary and are generally unevenly distributed. Total porosity of these samples ranges from 2.8% to 24.4 vol. % visible porosity. Petrophysical porosity and permeability of these samples vary from 2.5 to 24.8% and 0.1 to 1540 md, respectively.

Samples assigned to Reservoir Facies 1 generally display comparable grain sizes, varying from coarse grained to pebble-grade. Variations in reservoir quality also appear to be controlled by variations in grain size, sorting, kaolinite formation, quartz overgrowths and localized carbonate cements.

Samples assigned to Reservoir Facies 2 are generally lower coarse grained to fine grained, with smaller pore sizes than those observed in Reservoir Facies 1. Pores are spatially distributed, with common oversized pores. Overall the tendency is for reservoir quality to be better than Reservoir Facies 1. Variations in reservoir quality also appear to be controlled by variations in kaolinite formation, quartz overgrowths and localized carbonate cements, the same as Reservoir Facies 1.

Samples assigned to Reservoir Facies 3 and 4 are mostly of finer grain sizes, generally with high total clay matrix content. The general decrease in reservoir quality in these samples can be attributed to extensive carbonate cementation, along with the combined effects of dispersed clay and kaolinite distribution.

Total porosity, comprising primary, secondary, and microporosity, varies from negligible to very good. Pore types comprise mainly secondary dissolution porosity, with lesser microporosity and primary intergranular pores. Dissolution porosity is mainly recognized by the presence of oversized pores, and by partially leached carbonate cements (mainly ferroan calcite). Dissolution of unstable feldspar grains is thought to have been a major factor in secondary porosity development. Many oversized pores are partially filled with authigenic kaolinite. Microporosity, occurring in-between clay platelets, may be

underestimated in the point count analysis due to its minute size. Thin section study revealed that the main porosity in the samples is secondary, derived from the leaching of detrital feldspars. Most sandstones contain minor to trace intergranular porosity that is probably primary in origin. Porosity distribution is generally uneven in this suite of samples. The difference between point counts and helium porosity values can be attributed to microporosity in clay minerals.

6. Reservoir Permeability Prediction

The permeability prediction model will be based on an integration of wireline logs and core data combine with the reservoir facies characterization to generate the permeability prediction model for each reservoir facies. Core porosity and permeability will be used as a main data set for generating the permeability prediction model. The grouping of permeability is defined by reservoir facies type and the permeability prediction model is derived from the regression linear equations.

A cross plot of core porosity and permeability from all wells (Figure 5), colored by reservoir facies type, shows good relationship between porosity and permeability with overall coefficient of determination is 0.81. The porosity and permeability cross plot also show different trends with different permeability prediction equations from each reservoir facies.

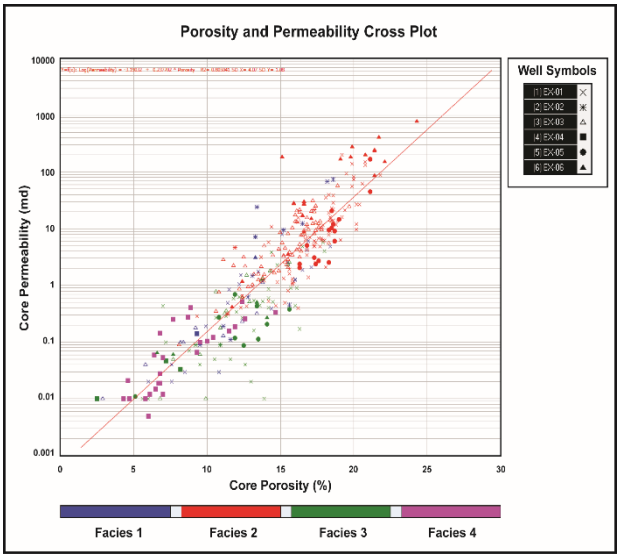

Figure 5 A cross plot of core porosity and permeability from all wells, colored by reservoir facies type.

In the reservoir facies 1, Conglomerate and conglomeratic sandstone, core porosity and permeability cross plot (Figure 6A) shows a good correlation, with a coefficient of determination of 0.75. Overall data points align with the average trend line and range from low to medium-high poro-perm values (from 2.9% porosity with permeability 0.01 md up to 18.6% porosity with permeability 74.2 md).

In the reservoir facies 2, Fining upward cross-bedded sandstone, the core porosity and permeability cross plot (Figure 6B.) shows good correlation with a coefficient of determination of 0.67. Overall, data points are aligned with the average trend line and are slightly higher than the trend line of reservoir facies 1. Most of the data points range across the medium to high poro-perm values (from 8% porosity with permeability 0.5 md up to 24.8% porosity with permeability 1090 md).

In the reservoir facies 3, Interbedded sandstone and siltstone, the core porosity and permeability cross plot (Figure 6C.) shows a fair correlation with a coefficient of determination of 0.57. Most of data points are located lower than the average trend line (with significantly lower positions than the trend line of reservoir facies 1 and 2). The data point distribution is mainly in the range covered by low to medium poro-perm values (from 2.5% porosity with permeability 0.01 md up to 18% porosity with permeability 4.05 md).

In the reservoir facies 4, Coarsening upward alternating sandstone and siltstone, the core porosity and permeability cross plot (Figure 6D.) shows agood co rrelation with a coefficient of determination of 0.63. Overall data points align with the average trend line, however the trend line of this reservoir facies is positioned lower than the average trend line, the same as reservoir facies 3 (which is significantly lower than the trend lines of reservoir facies 1 and 2).

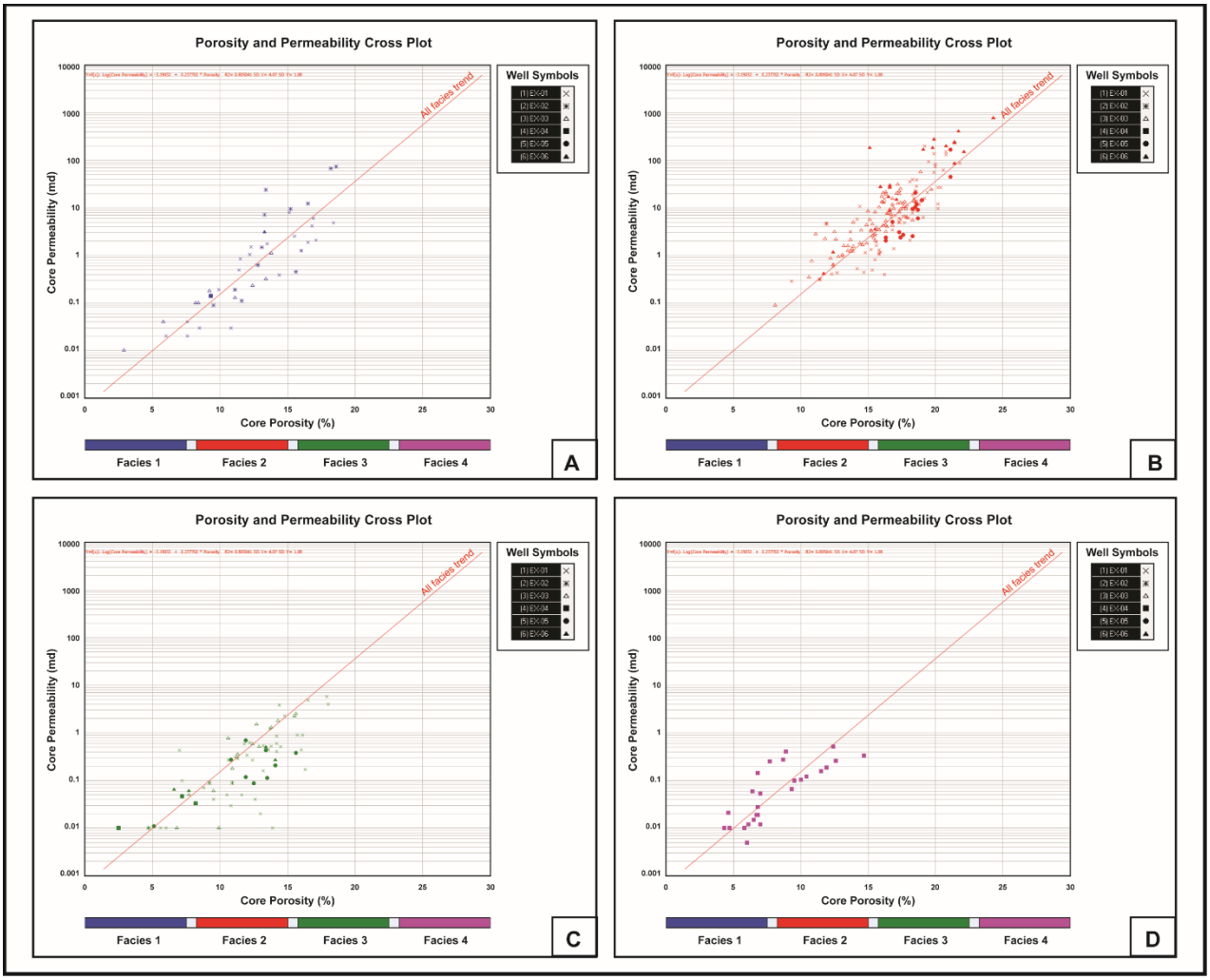

Figure 6 Cross plots of core porosity and permeability from all wells subdivided by facies A) Conglomerate and conglomeratic sandstone, B) Fining-upward cross-bedded sandstone, C) Interbedded sandstone and siltstone, D) Coarsening-upward alternating sandstone and siltstone.

Most of the data points range across low to medium-low poro-perm values (from 4.3% porosity with permeability 0.01 md up to 14.7% porosity with permeability 0.331 md).

Summary of the permeability prediction model of each reservoir facies with permeability prediction equation and coefficient of determination are presented in Table 1.

Facies	Equation	R^2	SD	
			X	Y
1	Log(Permeability) = -2.99951+0.224649*Porosity	0.747906	3.70	0.96
2	Log(Permeability) = -2.79780+0.220188*Porosity	0.665024	2.63	0.71
3	Log(Permeability) = -2.66619+0.168803*Porosity	0.570176	3.32	0.74
4	Log(Permeability) = -2.69386+0.176086*Porosity	0.633836	2.74	0.61
All	Log(Permeability) = -3.19032+0.237702*Porosity	0.805041	4.07	1.08

Table 1 Summary of the permeability prediction model of each reservoir facies with permeability prediction equation and coefficient of determination.

The results from permeability prediction model based on wireline logs calibrated between predicted permeability values and actual permeability values (core permeability) show that the overall coefficient of determination is 0.40 (from linear regression). Predicted permeability plots using actual permeability measures (Figure 7) shows a good relationship to the predicted permeability curve (red-colored log curve) it is generally aligned with the actual permeability measures from the core plugs (blue-colored dots).

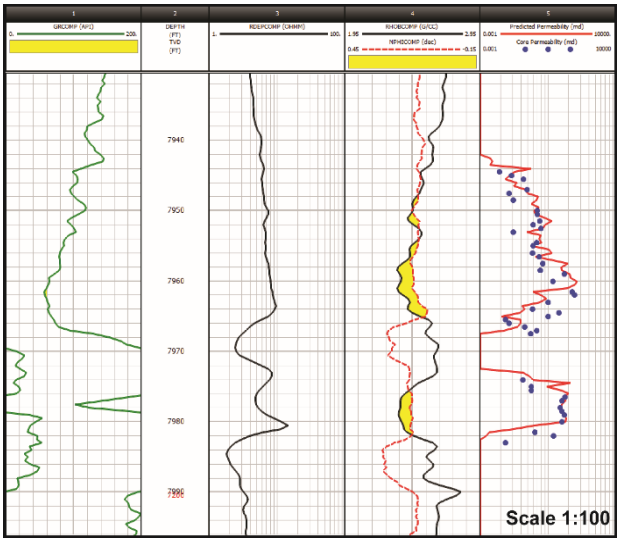

Figure 7 Wireline log plot shows good relationship of predicted permeability curve (red-colored log curve) that is quite aligned with the actual permeability from the core data (blue-colored dots).

A cross plot of predicted permeability and actual permeability (Figure 8), colored by reservoir facies type, shows and overall fair to good relationship. In the reservoir facies 1, the result shows a scattering of data points with fair relationship between predicted and actual permeability (Figure 9A). Observations in this facies show some portions of the predicted permeability curve is significantly lower than the actual permeability. This may be due to higher density readings in the bottom sand. In the reservoir facies 2, the result shows a grouping of the data point located at medium to high permeability values, with some being more scattered than others. The relationship of predicted and actual permeability is better than for reservoir facies 1 (Figure 9B). In the reservoir facies 3, the result shows a grouping of the data points located at low to medium permeability values, with the best relationship between predicted and actual permeability when compared to other facies (Figure 9C). In the reservoir facies 4, the result shows a grouping of the data point located at low permeability values, with a fair relationship between predicted and actual permeability. Observations in this facies show the predicted permeability is significantly lower than the actual permeability. This implies that the wireline porosity is typically lower than core porosity as core plug collection was biased toward sandier units (Figure 9D).

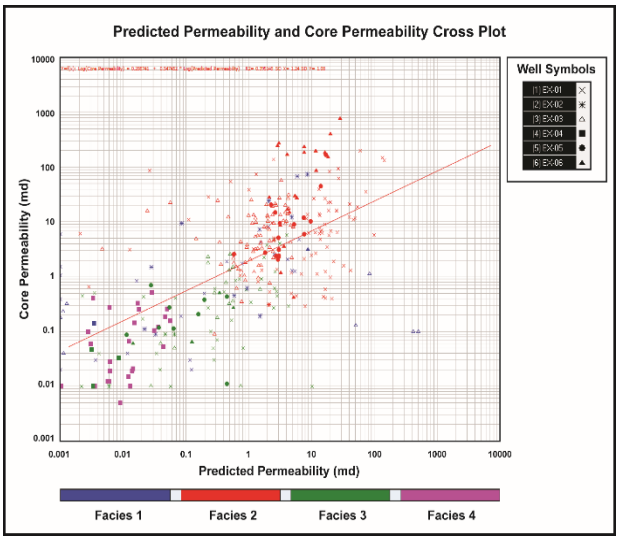

Figure 8 A cross plot of predicted permeability and actual permeability (from core) from all wells, colored by reservoir facies type, shows overall fair to good relationship.

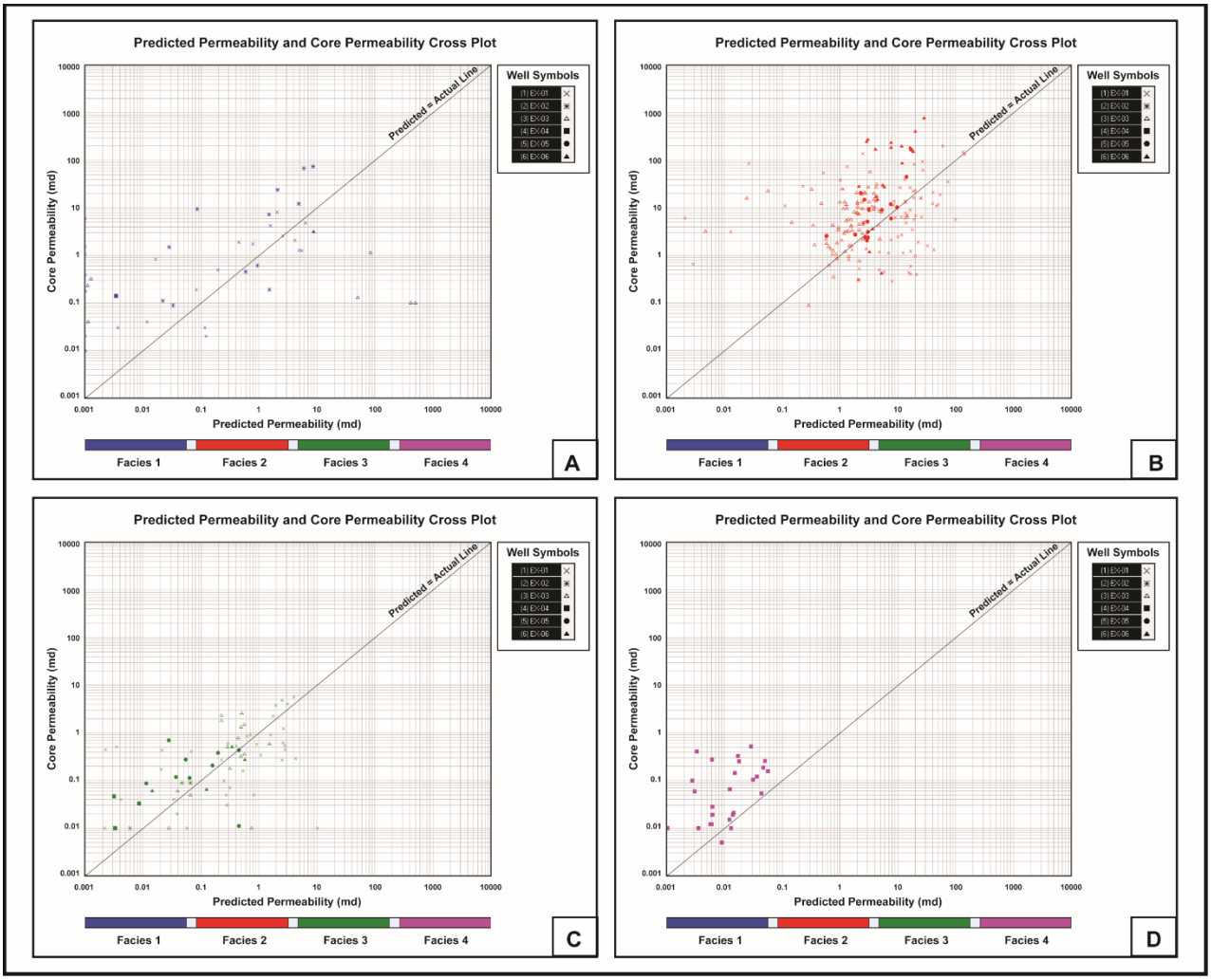

Figure 9 Cross plot of predicted permeability and actual permeability (from core) from all wells divided by facies A) Conglomerate and conglomeratic sandstone, B) Fining-upward cross-bedded sandstone, C) Interbedded sandstone and siltstone, D) Coarsening-upward alternating sandstone and siltstone.

7. Production Result Validation

Production performance validation is used to quantify the performance of reservoir sand at a fieldwide scale, while core-based models test the reservoir quality at the inter-well scale. In this study, actual reservoir production performances are available from 44 single perforated sands that can be used to evaluate the success of permeability prediction models at a fieldwide scale.

There are three definitions of reservoir flow performance in use, namely; no-flow, low-flow and high-flow. These relate to the actual production flowrate. From 44 single perforated sands, there are 4 sands defined as no flow, 12 sands defined as low flow, and 28 sands defined as high flow, based on the predicted permeability cutoff. The actual production performance validation shows overall success rate of permeability prediction by using studied models is 56.82%. For the individual reservoir flow performance type, the success rate of no flow prediction is 16.76%, the success rate of low flow prediction is 30.00%, and the success rate of high flow prediction is 75.00% as shown in Figure 10.

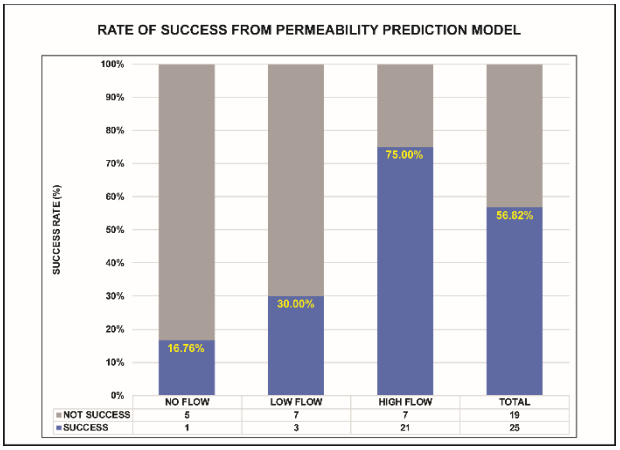

Figure 10 Bar graph chart shows rate of success from permeability prediction by using studied models divided by reservoir flow performance type.

The result validates the application of the permeability prediction model from cored wells to predict reservoir permeability in non-cored wells with similar geological settings. However, the result also shows poor prediction results in no-flow and low-flow reservoir performance type. It can be concluded that the high reservoir flow efficiency grouping more reliably predicts reservoir flow performance using predicted permeability curves compared to the low reservoir flow efficiency grouping.

8. Conclusions

There are four reservoir facies defined in the southern area of Pattani basin namely 1.) Conglomerate and conglomeratic sandstone, 2.) Fining-upward, cross-bedded sandstone, 3.) Interbedded sandstone and siltstone, and 4.) Coarsening-upward, alternating sandstone and siltstone, with two associated facies defined as non-reservoir facies, that are non-marine shale and marginal marine shale.

Based on petrographic study of reservoir facies, most of reservoirs in the study area are sandstone reservoirs. The sandstones are mainly classified as sublitharenite, feldspathic litharenite, subarkose and litharenite. The framework grains are mostly quartz with minor to common feldspar and minor to very common lithic fragments with minor accessory grains, such as muscovite and heavy minerals. Cements identified in these sandstones are calcite (mainly ferroan), dolomite, siderite, quartz overgrowths, pyrite, kaolinite, and pore-lining to pore-filling undifferentiated clay. Clay fraction XRD analyses show kaolinite and mixed-layer illite/smectite to be the dominant clay minerals in the study area. The reservoir quality of the sandstone samples appears to be very poor to very good. Pores are mostly secondary and are generally unevenly distributed. Petrophysical porosity and permeability of these samples vary from 2.5 to 24.8% and 0.1 to 1540 md, respectively.

Porosity and permeability controls, based on petrographic study of reservoir facies, show that porosity and permeability have been significantly reduced by compaction, authigenic kaolinite, ferroan calcite and quartz overgrowths. Locally, sideritic and pyrite cement have also reduced porosity and horizontal permeability. Following deposition, compaction reduced porosity by increasing the density of grain packing, as indicated by the mainly planar grain contacts. Variation in grain size also affects reservoir quality. Larger grains tend to have larger associated pore throat sizes and therefore better permeability. Locally, poor sorting has resulted in tighter grain packing, causing permeability reduction. Dissolution of feldspar, ferroan calcite and other cements have enhanced porosity after compaction and silica cementation. This has often resulted in the merging of adjacent dissolution pores, enhancing pore-interconnectivity. However, this increase in porosity and permeability has been partially offset by the formation of authigenic kaolinite, reducing macroporosity and forming microporosity. This has effectively reduced permeability by increasing pore tortuosity and decreasing mean pore throat radii. The results from permeability prediction model based on wireline logs calibrated between predicted permeability values and actual permeability values (core permeability) show overall coefficient of determination is 0.40 (from linear regression) with predicted permeability plot with actual permeability in wireline logs showing a good relationship between predicted permeability and actual permeability from the core data.

The result validates the application of the permeability prediction model from cored wells to predict reservoir permeability in non-cored wells with similar geological settings. However, the result also shows poor prediction results in no-flow and low-flow reservoir performance type, it may be implied that with the high reservoir flow efficiency grouping it is easier to predict the reservoir flow performance by using predicted permeability than it is in zones of low reservoir flow efficiency.

Based on the results of this study, there are many factors that control on reservoir permeability. It difficult to predict the reservoir permeability by using only one petrophysical property such as porosity (in this study) thus integration of all petrophysical properties is needed for more accurate permeability prediction. Moreover, the understand of reservoir petrography, including diagenetic events across study area, is fundamental in generating the best fit model for permeability prediction. However, the results of this study still show a positive result in terms of a permeability prediction model, supported by overall success rate of permeability prediction, as using the study models there is a more than 50% success rate.

9. Acknowledgements

I would like to thank to Chevron Thailand Exploration and Production for permission to use the data, including core, wireline logs, and production performance data and for the opportunity and scholarship to study Master Degree of Petroleum Geoscience at Chulalongkorn University. I also would like to express my very great appreciation to my supervisor, Professor Dr. John K. Warren for his excellent suggestions, supervision and encouragement throughout my research work. Also, the special appreciation is expressed to all Chevron staff, especially in Department of Reservoir Management.

10. References

Chaiwan, P., 2010, Building a core-calibrated wireline-based permeability prediction model for Ubon field, Thailand, with model testing in uncored well sections and validation by TST or DST, Master's thesis, Chulalongkorn University, Thailand, 80 p.

Jardine, E.,1997. Dual Petroleum systems governing the prolific Pattani Basin, off-shore Thailand, Proceedings of the Petroleum Systems of SE Asia and Australia Conference, Jakata, May 21-23, 1997, p. 351-363.

Lockhart, B.E., Chinoroje, O., Enomoto, C.B., and Hollomon, G.A., 1997. Early Tertiary deposition in the southern Pattani Trough, Gulf of Thailand, Proceeding of the International Conference on the Stratigraphy and Tectonic Evolution of Southeast Asia and the South Pacific, Bangkok, August 19-24, 1997, p.476-489.

Narapan, J., 2015, Different types of organic-rich geological markers in South Pailin field, Pattani Basin, Gulf of Thailand, Master's thesis, Chulalongkorn University, Bangkok, 51 p.

Watcharanantakul, R. and Morley, C.K., 2000, Syn-rift and post-rift modelling of the Pattani Basin, Thailand: evidence from a ramp-flat detachment: Marine and Petroleum Geology, v. 17, p. 937-958.